

Article

Evidence for the Root-Uptake of Arsenite at Lateral Root Junctions and Root Apices in Rice (*Oryza sativa* L.)

Angelia L. Seyfferth^{1,*} , Jean Ross² and Samuel M. Webb³¹ Department of Plant & Soil Sciences, University of Delaware, Newark, DE 19716, USA² Delaware Biotechnology Institute, University of Delaware, Newark, DE 19711, USA; jeanross@udel.edu³ Stanford Synchrotron Radiation Lightsource, Menlo Park, CA 94025, USA; samwebb@slac.stanford.edu

* Correspondence: angelias@udel.edu; Tel.: +1-(302)-831-4865; Fax: +1-(302)-831-0605

Received: 12 July 2017; Accepted: 11 August 2017; Published: 14 August 2017

Abstract: The uptake of arsenite (As(III)_i) at the Casparian band via *Lsi1* and *Lsi2* Si transporters is responsible for ~75% of shoot As(III)_i uptake in rice and, therefore, ~25% of shoot As(III)_i is taken up by other transport pathways. We hypothesized that areas devoid of Casparian bands—lateral root junctions and root apices—can transport As(III)_i into roots. We analyzed the elemental distribution and As concentration, speciation, and localization in rice roots from soil-grown and solution-grown plants. With solution-grown plants dosed with As(III)_i , we sectioned roots as a function of distance from the root apex and analyzed the cross-sections using confocal microscopy coupled to synchrotron X-ray fluorescence imaging and spectroscopy. We observed elevated As(III)_i associated with lateral root junctions and root apices in rice. As(III)_i entered the stele at lateral root junctions and radially permeated the root interior in cross-sections 130–140 μm from the root apex that are devoid of Casparian bands. Our findings suggest that lateral root junctions and rice root apices are hot-spots for As(III)_i transport into rice roots, but the contribution to shoot As requires further research.

Keywords: rice; arsenite; transport; synchrotron XRF imaging

1. Introduction

Arsenic (As) is phytotoxic and its uptake by rice roots affects rice yield [1,2]. Furthermore, its storage in grain is a detriment to human health worldwide, particularly for populations already exposed to As through drinking water [3,4]. Four major chemical species of As have been detected in rice paddy porewaters and include the acutely toxic inorganic species arsenite (As(III)_i ; H_3AsO_3^0 at circumneutral pH) and arsenate (As(V)_i ; H_2AsO_4^- or HAsO_4^{2-} at circumneutral pH) and the organic species monomethylarsonous acid (MMA) and dimethylarsinic acid (DMA). Each of these species are transported into rice root cells due to their chemical similarities (i.e., hydrated radius and valence) to plant nutrients: As(V)_i is analogous to inorganic phosphate (P_i) and shares the P_i transport pathway [5], whereas As(III)_i and to some extent DMA and MMA are analogous to silicic acid [6,7]. While management practices affect pore water speciation [8,9], the dominant As species in typical flooded paddy porewater is As(III)_i [10]. It is, therefore, imperative to understand the mechanisms and pathways by which As(III)_i is transported into rice roots and ultimately stored in grains to effectively minimize the negative impacts of As on rice and humans.

The prevailing view of As(III)_i uptake in rice is that it occurs principally at the Casparian bands via *Lsi1* and *Lsi2* Si transporters [6,11]. Casparian bands are highly suberized deposits in the cell walls that surround both the exodermis and the endodermis and prevent the passive flow of solutes and water into the vasculature [12,13]. Ma et al. [6] clearly showed that knocking out *Lsi1* and particularly *Lsi2* transporters in rice mutants significantly decreased As tissue concentrations in plants exposed

to As(III)_i in hydroponic media; however, mutants still contained appreciable As in shoots. Shoot As concentrations were lowered by approximately 32–72% in *Lsi1* knockouts and 36–72% in *Lsi2* knockouts compared to that of wild type depending on exogenous Si supply [6]. These results suggest that while *Lsi1* and *Lsi2* undoubtedly play a large role in As(III)_i root-uptake by rice and account for as much as ~75% of shoot As, additional As(III)_i root-uptake mechanisms exist.

Plant roots are developmentally and morphologically diverse, and it is well known that Casparian bands are not present in all root zones. Enstone and Peterson [14] described three distinct anatomical zones of growing roots that differ in the extent of Casparian band formation: (1) the immature root apical region where Casparian bands have not yet formed; (2) an intermediate region farther away from the apex where the endodermal Casparian band has formed but not the exodermal band; and (3) a mature region farthest from the apex where both Casparian bands have formed (for plants that have an exodermis, like rice). In addition, lateral roots emerge from the pericycle or endodermis in rice and must break through several layers of tissues [15], creating a potentially direct route of apoplastic entry into the vasculature. It is well known that Casparian bands are not present in root apices [16] or endodermal cells adjacent to lateral roots [17]. Could lateral root junctions and root apices that are devoid of Casparian bands be important for apoplastic transport of As(III)_i into roots?

The question of whether plant root zones devoid of Casparian bands can transport As(III)_i has received limited attention. Advanced imaging techniques used by different researchers have revealed elevated levels of As [18–21] or Se (as selenite) [22] associated with rice root apices where the Casparian bands are purportedly absent [12,13]. However, because some of these images [18,19] were generated from whole root mounts and not cross-sections, it was unclear if the elevated As signal in those studies was predominantly on the inside of the roots or on the outside of roots associated with Fe plaques (or both). Other researchers have successfully used computed tomography or modeling approaches to estimate the influx of As in root apices in rice, wheat, and cowpea roots in short-term studies [20,23]. Ma et al. [24] demonstrated that lateral roots are important for Si transport in rice, but the importance of these zones for As(III)_i root-uptake has only recently been investigated [25].

We posit that lateral root junctions and root apices are hot-spots for As(III)_i transport into rice roots. To test this, we analyzed the elemental distribution and As concentration, speciation, and localization in rice roots from soil-grown and solution-grown plants. With solution-grown plants exposed to 6.7 μM As(III)_i for six weeks, we sectioned roots as a function of distance from the root apex and analyzed the sections using confocal microscopy and synchrotron X-ray fluorescence imaging techniques. The localization of elevated As(III)_i reaching the vascular tissue at lateral root junctions and the radial penetration of reduced As throughout the root interior of apical tissues devoid of Casparian bands 130 μm from the root tip and localized to the stele 500 μm from the tip provide evidence that some As(III)_i is transported into roots in these zones. The results presented here show that As(III)_i transport into root zones free of Casparian bands can occur.

2. Results

2.1. Arsenite Uptake at Lateral Root Junctions

Lateral root junctions appeared to be hotspots for As(III)_i entry into the vascular tissue (Figure 1). A soil-grown rice root without visible Fe plaque coatings was utilized for micro-X-ray fluorescence (μXRF) imaging analysis. This root was not coated in an Fe plaque, but visible reddish-orange deposits at all of the lateral root junctions were observed (data not shown) that were elevated in Fe and As (Figure 1a,b). Higher resolution images revealed that As(III)_i was more abundant than As(V)_i and that As(V)_i was associated with the Fe (Figure 1c–f). In contrast, As(III) (inclusive of free arsenite and arsenite bound to S) penetrated deeper into the root interior than Fe and As(V)_i and was deposited into the stele from the lateral root, similarly to K (Figure 1f,g). This As(III) was likely free As(III)_i as it was not co-located with S (Figure 1h).

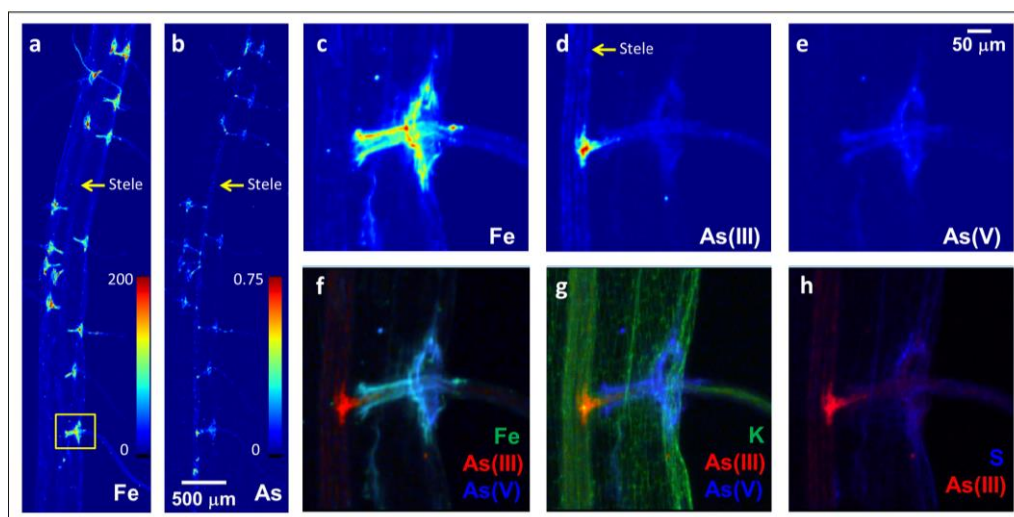


Figure 1. Two-dimensional X-ray fluorescence image of total Fe (a) and As (b) in a whole mount of a Fe plaque-free rice root grown in well weathered soil. Panels (c–h) are higher resolution images of the yellow box in panel (a) that show the Fe (c), arsenite (As(III)) (d), and arsenate (As(V)_i) (e) distribution where a lateral root has formed from the main root, and panels (f–h) are tricolor plots that show the localization of As(III) in relation to As(V)_i and Fe (f), K (g), and S (h). All colormap units are in pg cm^{-2} , with a maximum of 200 for Fe and 0.75 for As, and show that lateral root junctions are hotspots of As(III)_i entering the vascular tissue.

2.2. Arsenite Uptake Rice Root Apices

Soil-grown rice roots also contained elevated Fe and As concentrations in root apices relative to that of more mature neighboring root regions (Figure 2). Fe concentrations were $\sim 5\times$ higher in root apices than in neighboring more mature regions (Figure 2a). Similarly, As concentrations were $\sim 5\times$ higher in root apices than in neighboring root regions and consisted of mainly reduced As as As(V)_i was not detected (Figure 2b,c). These data do not readily reveal whether the elevated As(III)_i and Fe found in root apices is on the outside associated with Fe plaques or on the inside of the root tissues. We, therefore, further examined the potential for As(III)_i transport at root apices by utilizing a hydroponic approach to obtain root tissues for cross-sectional analysis.

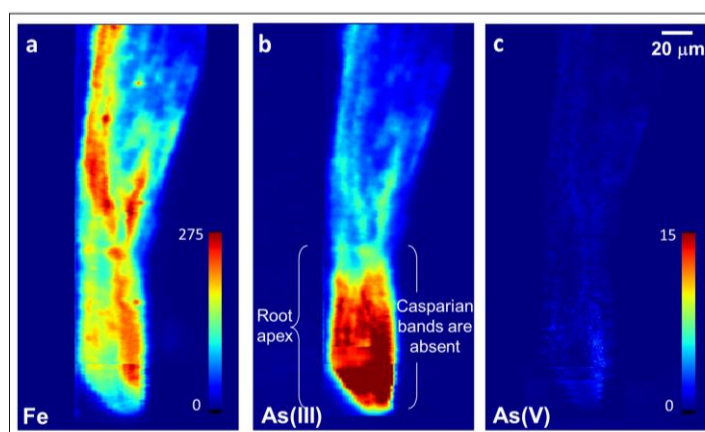


Figure 2. Two-dimensional X-ray fluorescence image of total Fe (a), As(III) (inclusive of free arsenite and arsenite bound to S) (b), and As(V)_i (c) in a whole mount of a soil-grown rice root tip exposed to elevated As in well-weathered soil and harvested at plant maturity. Colormap units are in pg cm^{-2} , with maximum of 275 for Fe and 15 for As, and show highest As in the root apices as As(III).

To examine whether the elevated As we observed in root apices (Figure 2) was localized to the root interior or exterior, we grew rice in hydroponic culture (Table 1) and exposed plants to 6.7 μM As(III)_i for six weeks in order to obtain materials for detailed root sectioning and microspectroscopic analysis. We developed a novel and systematic approach where fresh roots were embedded in freezing media and slam-frozen between liquid nitrogen-cooled copper blocks before sectioning the roots as a function of distance from the root tip, and alternate slices were placed on glass or quartz slides for confocal microscopy or μXRF imaging, respectively. The novelty lies in the whole approach but specifically in using mirror image slices of sections for synchrotron and confocal imaging. The slam-freezing method has an advantage over flash-freezing or freeze-drying in that ice crystals do not form and, therefore, no to minimal sample distortion occurs as observed by the well-preserved ultrastructure (Figures 3 and 4). Results from solution-grown rice dosed with 6.7 μM As(III)_i clearly show elevated As that permeated the root interior in less mature regions 130 μm from the apex (Figure 3) compared to that seen in the more mature regions 500 μm from the apex (Figure 4). With both confocal (Figure 3a) and epifluorescence (Figure 3e) microscopic imaging of the less mature root region, no discernable Casparian bands on the endodermis or exodermis were observed. In this region, As permeated through the entire root interior and was present predominantly as reduced As (Figure 3b–d). Like reduced As, S also permeated through the entire root interior in less mature apical regions, but not Fe and Ca (Figure 3f–h).

In contrast to the less mature root region, the more mature root region 500 μm from the apex exhibited more cell differentiation and visible Casparian bands at the endodermis and exodermis as revealed by both confocal (Figure 4a) and epifluorescence (Figure 4e) microscopy. This more mature root region had ~60–80% less As in the root interior than in the less mature apical region (Figures 3b and 4b) and most of it was as As(III) localized to the stele (Figure 4c,d). A visible ring of Fe but not Ca at the endodermis was pronounced (Figure 4f,g). The localization pattern of S was similar to that of As(III) except in procambium where As(III) was abundant (Figure 4h).

The differences in localization of chemical species between less mature and more mature root portions are more visible with tricolor images plotted on the same intensity scale (Figure 5). In the mature root region, most of the As(III) is visible in the stele and appears partially co-localized with S but not Ca (Figure 5a,b). In the less mature root region, in contrast, As(III) is in much higher concentration throughout the root interior and it appears to be co-localized with S but not Ca (Figure 5a,b). Correlation plots between Fe, S, or Ca vs. As(III) fluorescence signal intensity show distinct zones where the relations between species differ for the differentiated mature root portion (Figure 6a–c) to a greater extent than the less mature root portion (Figure 6d–f).

Table 1. Composition of chelator-buffered nutrient solution for the hydroponic rice experiment.

Hydroponic Component	Concentration in 8 L pot (μM)
Ca(NO ₃) ₂ ·4H ₂ O	1900.0
KNO ₃	1000.0
MES	1000.0
MgSO ₄ ·7H ₂ O	500.0
NH ₄ NO ₃	100.0
KH ₂ PO ₄	80.0
HEDTA	57.7
H ₄ SiO ₄	50.0
FeCl ₃ ·6H ₂ O	20.0
H ₃ BO ₃	10.0
ZnCl ₂	8.0
CuCl ₂ ·2H ₂ O	2.0
MnCl ₂ ·4H ₂ O	0.6
NiCl ₂ ·6H ₂ O	0.1
Na ₂ MoO ₄ ·2H ₂ O	0.1

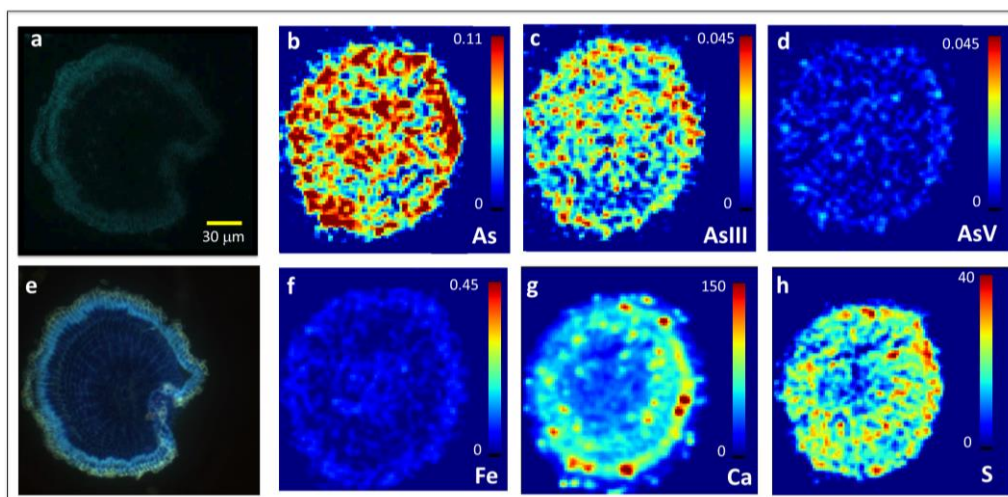


Figure 3. Images of 10 μm thin cross-sections of hydroponically-grown rice roots exposed to 6.7 μM As(III)_i taken 130–140 μm from the root apex in the less mature root region and showing radial penetration of reduced As throughout the root interior in the region where Casparian bands have not yet formed. (a) Confocal microscopy, (b–d,f–h) micro-X-ray fluorescence (μXRF) imaging, (e) epifluorescence microscopy after staining with berberine hemisulfate. Colormap units for Fe and As are in pg cm^{-2} (b–d,f), and are in fluorescence signal intensity for Ca (g) and S (h). Note that the root section for confocal and epifluorescence microscopy was distorted during its placement on the slide (Figure 2a,e), but not on the mirror image sections used for μXRF (Figure 2b–d,f–h). As(III) is inclusive of free arsenite and arsenite bound to S.

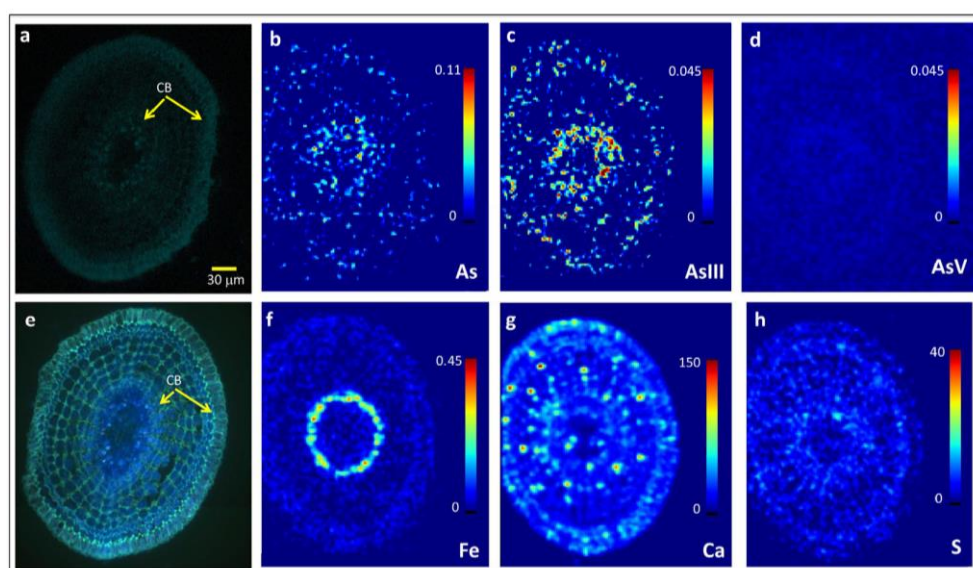


Figure 4. Images of 10 μm thin cross-sections of hydroponically-grown rice roots exposed to 6.7 μM As(III)_i taken 500–510 μm from the root apex in the more mature root region and showing restriction of radial As penetration. (a) Confocal microscopy, (b–d,f–h) μXRF imaging, (e) epifluorescence microscopy after staining with berberine hemisulfate. Colormap units for Fe and As are in pg cm^{-2} (b–d,f), and are in fluorescence signal intensity for Ca (g) and S (h). CB = Casparian bands on the exodermis and endodermis. As(III) is inclusive of free arsenite and arsenite bound to S.

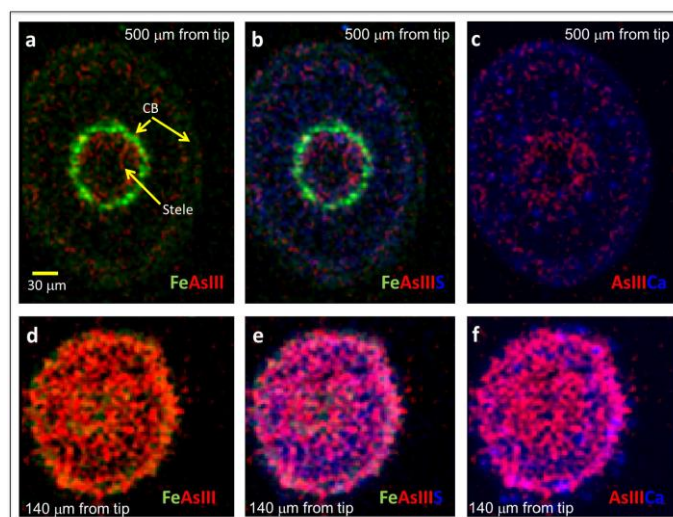


Figure 5. μ XRF bi- and tri-color images showing Fe, As(III), and S localization in 10 μ m thin cross-sections of hydroponically-grown rice roots exposed to 6.7 μ M As(III)_i and taken 500 μ m from the root apex (a–c) or 140 μ m from the root apex (d–f). CB = Casparian bands on the exodermis and endodermis. As(III) is inclusive of free arsenite and arsenite bound to S.

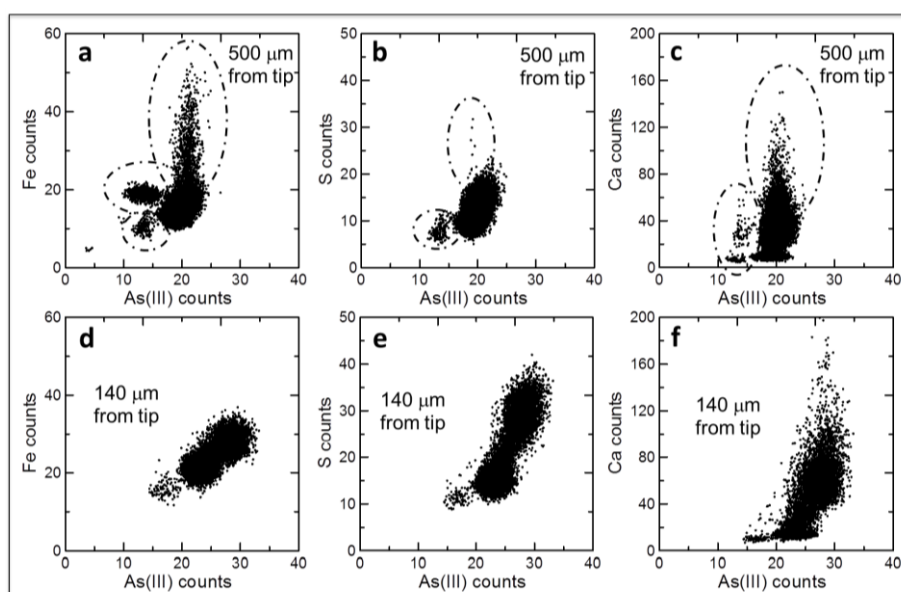


Figure 6. Correlation plots of fluorescence intensity counts of As(III) and Fe (a,d), S (b,e) and Ca (c,f) from μ XRF images shown in Figure 4. Cell differentiation in more mature root zones leads to differences in localization between As(III) and Fe, S, or Ca, examples of which are depicted by dashed ovals in (a–c). In contrast, little to no differences in elemental localization exist in less differentiated root zones closer to the root apex (d–f).

3. Discussion

To test whether As(III)_i transport in rice could occur at lateral root junctions and root apices, we analyzed the elemental distribution and As concentration, localization, and speciation in rice roots exposed to As. We observed elevated As as As(III)_i along lateral roots and into the stele at lateral root junctions whereas Fe and As(V)_i did not enter the stele (Figure 1). Our data do not reveal whether this transport was passive or active but the former seems more likely. As(III)_i is a neutral molecule at circumneutral pH (H_3AsO_3 , $pK_a = 9.2$) and is more conducive to passive transport than the

charged As(V)_i molecule. Furthermore, at typical rhizospheric pH < 6, As(III)_i has less of an affinity than As(V)_i to adsorb onto poorly crystalline iron oxides [26] that dominate Fe precipitates on rice roots [27–29] and were observed at the lateral root junctions in these samples. Lateral roots have been shown to contribute to Si uptake in rice [24], which is chemically analogous to As(III)_i. Recent work by Chen et al. [25] showed that OsNIP3;2—a membrane-bound intrinsic protein—is localized to lateral roots and plays a role in As(III)_i passive transport in rice roots. Our data provide additional evidence that lateral roots play a role in As(III)_i transport to the vasculature.

We further observed As as As(III) (inclusive of free As(III)_i and that bound to S compounds) in the less mature root region (<150 μm from root apex) of a whole-root mount of rice roots grown in As-rich soil (Figure 2). The elevated As(III) we observed in the less mature root apex corroborate previous findings that show elevated As [18–21] or Se (as selenite) [22] localized to apical regions in rice. However, the image (Figure 2) alone does not reveal whether the elevated As in apical regions equates to transport into the root interior because the image is a 2-D projection of a 3-D root. The depth of penetration of the X-rays in this C-rich material would allow the fluorescence photons from elements associated with the front surface, the interior, and the back surface of the root to be counted by the detector. Our results showing elevated Fe and As(III) in the less mature root apical region of whole-root mounts (Figure 2) could reflect As associated with Fe plaques on the root exterior. However, the enhanced uptake of Fe at the root apex of graminaceous species has been established [30,31]; thus, the elevated Fe we observed at root apices of whole root mounts (Figure 2) could reflect Fe uptake at the apical region. We, therefore, conducted additional experiments using hydroponic culture to examine the cross-sectional localization of Fe and As species as a function of distance from the root tip.

The coupled confocal and microspectroscopic analyses of root cross-sections revealed elevated As(III) that radially penetrated the root interior in the less mature apical region where Casparian bands were absent, whereas As was less abundant and localized to the stele in the more mature root region where Casparian bands were present (Figures 2–4). At the root apex, the Casparian band is not fully developed and is a zone allowing apoplastic flow into the stele [16]. Similar results were shown for selenite in rice where plants exposed to 1 μM selenite in hydroponic media concentrated selenite in apical regions 50–500 μm from the root apex [22]. The same group also provided evidence for the passive transport of selenite into the stele of cowpea roots within 2 mm of the apex and suggested that excretion of chelators in that region may complex selenite and aid in its entry into the vasculature [32]. While chelation and uptake could be possible for As(III)_i influx at the root apex (Figure 3), the differences in chemical behavior between arsenite and selenite in the rhizosphere suggest that their root entry at apices may result from different mechanisms.

The entry of As(III)_i into the vasculature in root regions of rice devoid of Casparian bands may behave similarly to that of water. At pH < 9, As(III)_i is a neutral molecule whereas most other mineral nutrients and inorganic contaminants are charged ions (e.g., selenite resides as a mixed phase of HSeO₃[−] and SeO₃^{2−} oxyanions at pH 5–8). Unlike ions, small neutral molecules are less restricted to passive radial transport. It has been established that water transport into roots is predominantly apoplastic when transpiration is high and that aquaporins in the transcellular path function to uptake water in more mature, suberized root regions such as those where Casparian bands have fully developed [33]. It is thus possible that As(III)_i is transported passively with transpirational water flux in rice root apices and this mechanism does not involve the cooperative Lsi1 and Lsi2 transporters. The *Lsi1* and *Lsi2* transporters have low expression at the root apical regions within 10 mm of the root tip, whereas *Lsi6*, a homologue of *Lsi1*, is highly expressed [34,35]. Yamaji et al. [34] showed that *Lsi6* is also expressed in nodes and is responsible for influx into grain at the nodes in cooperation with an unknown active effluxer that is *Lsi2*-like, but is not *Lsi2*. While it is possible that *Lsi6* functions in conjunction with an *Lsi2*-transporter to uptake As(III)_i in rice root apices, passive transport into roots with water is also plausible.

What is the fate of As(III)_i that enters rice roots through lateral root junctions and apical regions? Kopittke et al. [20] demonstrated that As(III)_i is quickly complexed with glutathione (GSH) in rice

roots exposed to As(III)_i in hydroponic media. Using NanoSIMS, Moore and colleagues provided evidence for As co-localization with S in vacuoles within the pericycle for rice exposed to As(III)_i [36,37]. Although μ XRF does not provide as fine a resolution as NanoSIMS, our data partially corroborate this past work as we also observed co-localization of As(III) with S in the more mature root portion 500 μ m from the apex within or near the vascular bundle (Figure 4). As(III)-GSH complexes have limited transport to shoots compared to free As(III)_i, and, thus, they would not readily transport to shoots. However, in the less mature root region 140 μ m from the apex, the relationship between As(III) and S differs from the more mature root region (Figure 6). In the less mature root region and in lateral root junctions, As(III) was poorly correlated with S within the (pre)vascular cylinder (Figures 1 and 3) and this likely indicates the presence of more free As(III)_i there. Free As(III)_i is both xylem and phloem mobile [38,39]. Free As(III)_i that is transported to the stele in lateral root junctions and apical regions may access the (meta)xylem and ultimately be transported to shoots, including grain. While the total root volume available for apoplastic transport is relatively low (e.g., 5–30%), the mechanism could be significant for graminaceous species like rice. In rice, Lsi1 and Lsi2 transporters at the Casparian band are responsible for ~75% of shoot As [6], and, therefore, passive transport through lateral root junctions and rice root apices could potentially account for up to 25% of shoot As, although limited data are available in this regard and other mechanisms may be also important. Further work is required to quantify the importance of apoplastic As(III)_i uptake to shoot As in rice.

4. Materials and Methods

4.1. Soil Experiment

Full details on rice growth, sampling, and digestion of plant tissues for the soil experiment can be found in Seyfferth and Fendorf [40] and Seyfferth et al. [29]. Briefly, rice (*Oryza sativa* L. cv. M206) was grown under flooded conditions in As-contaminated soil and irrigated with As-contaminated water at a ratio of 80% As(III)_i and 20% As(V)_i with total As concentrations of 4 μ M, typical of paddy soil irrigated with moderately-contaminated groundwater [41]. Plants were grown to maturity in a controlled environment with 12 h light and dark cycles with maximum photosynthetic photon flux density of 600 μ mol m⁻² s⁻¹ and temperatures ranging from 25 °C to 28 °C. At harvest, roots were removed from soil, washed gently with 18 M Ω -cm distilled deionized (DDI) water, and placed in an anoxic chamber to dry under anoxic conditions. Roots were sealed in gas-impermeable boxes and transported to Stanford Synchrotron Radiation Lightsource (SSRL) and mounted on adhesive film for μ XRF imaging analysis.

4.2. Hydroponic Experiment and Root Sectioning

Rice (*Oryza sativa* L. cv. M206) seed was surface sterilized in dilute bleach solution and soaked for 24 h in deionized water before germinating on moistened germination paper. Plants were grown in a chelator-buffered nutrient solution consisting of macro- and micronutrients detailed in Table 1 and exposed to As concentrations of 6.7 μ M As(III)_i for six weeks. The nutrient solution was buffered with 2-(N-morpholino)ethanesulfonic acid (MES) adjusted to a pH of 6.5, and contained 57.7 μ M HEDTA (2-hydroxyethyl)ethylenediaminetriacetic acid), which is a 27.7 molar excess of the sum of micronutrients [42,43]. Nutrient solutions were changed every 3–5 days, with more frequent changes as the plants grew larger. Plants were grown in an environmental chamber (70% relative humidity, 28/22 °C day/night cycle) using growth lights (Lumigrow, Novato, CA, USA) set to a 16-h photoperiod with light intensity of 500 μ mol m⁻² s⁻¹.

At harvest, roots were separated from shoots and rinsed with DDI water to prepare roots for sectioning. We developed a novel and systematic approach to root freezing and cryosectioning where fresh roots were embedded in freezing media and slam-frozen between liquid nitrogen-cooled copper blocks before sectioning the roots as a function of distance from the root tip. Fresh root tissues were individually submerged in tissue freezing media (Electron Microscopy Sciences), and the hydrated

root structure was preserved by rapid freezing in between two liquid nitrogen-cooled copper blocks. Roots were sectioned at 10 μm intervals as a function of distance from the root apices using a Leica CM3050 S cryostat operated at $-28\text{ }^{\circ}\text{C}$. We developed a novel technique to create mirror images for both confocal and μXRF imaging analysis by collecting the first 10 μm section onto a glass slide for subsequent staining and confocal microscopy, and collecting the adjacent 10 μm section onto a quartz slide for μXRF imaging analysis. Samples for μXRF imaging analysis were placed into a gas-impermeable container with an oxygen scrubber during transport to SSRL. While many sections were examined with light microscopy (Zeiss Axioplan 2) to evaluate the structural integrity of the sections obtained, two sections were chosen to characterize fully: one 130–140 μm and another 500–510 μm from the root apex in less mature and more mature root zones, respectively.

4.3. Light Microscopy, Section Staining, and Confocal Imaging

Root cross-sections were checked for structural integrity using brightfield light microscopy with a Zeiss Axioplan 2. Each root thin-section on a glass slide that was selected for further analysis was stained using berberine-aniline blue, which illuminates the presence of Casparian bands [44]. Stained cross-sections 140 and 510 μm from the root apices were first imaged using epifluorescence microscopy with a Zeiss Axioplan 2. Then, the stained cross-sections were imaged on a Zeiss LSM 780 laser scanning confocal microscope with an EC Plan-Neofluar $40\times$ (NA = 1.3) oil immersion objective lens. Berberine-aniline blue was excited at 405 nm and a 410–585 nm emission range was collected. Image J was used to visualize confocal images.

4.4. μXRF Imaging and Spectroscopy

Whole root mounts from soil experiments and 10 μm cross-sections of roots from hydroponic experiments were analyzed for As species with μXRF imaging analysis at SSRL beam line 2–3 using Kirkpatrick-Baez mirrors to deliver microfocused X-rays at a nominal beam size of $2 \times 2\ \mu\text{m}$. The incident X-ray energy was selected using a Si(111) monochromator crystal, calibrated by assigning the first inflection point of the white line of sodium arsenate to 11,874.0 eV. Whole root mounts from the soil experiment affixed to adhesive film or unstained cross-sections on the quartz slides from the solution experiment were mounted onto an aluminum sample holder and placed 45° to the incident X-ray beam. At incident energies of 11,880, 11,874, and 11,871 eV, which correspond to total As, As(V)_i , and As(III)_i , respectively, fluorescence intensities of As as well as Fe, Ca, and S were monitored with a Vortex SDD detector. Overlap from neighboring elements was minimized by using narrow regions of interest (ROI) windows and monitoring Fe with the $k\beta$ line. The detector was placed 45° to the sample (90° to the incident beam) as the sample was rastered in the microbeam with a Newport stage utilizing the following step size and dwell time per pixel: 5 μm and 25 ms for the lateral root whole mount, 2 μm and 200 ms for the lateral root junction, 1 μm and 50 ms for the root apex whole mount, and 2 μm and 750 ms for the apical cross sections. After each scan, light microscopy was used to confirm no beam damage to the sample during imaging. Redistribution of elements upon drying is a possibility with dried thin sections, but was likely minimal in this study as evidenced by elemental differentiation that coincided with structural elements. Quantum Detectors Xspress3 pulse processing electronics were used to process the output of the detector. Fluorescence intensities were integrated over the appropriate regions of interest (ROI) and narrow ROI windows were utilized to minimize contamination from neighboring elements. A least-squares fit of the As images to normalized mu standard spectra at each mapping energy was performed to create chemical speciation maps of reduced As (targeting As(III)_i but may include As(III) associated with S) and oxidized As (As(V)_i) distributions [19]. Fluorescence signal intensities of As species and Fe were converted to concentrations for semi-quantitative analysis [28,29], whereas fluorescence signal intensities are reported for Ca and S. All images and correlation plots of signal intensities were processed using the MicroAnalysis Toolkit [45].

Acknowledgments: We thank Michael Hilyard for assistance with solution experiments and anonymous reviewers who have helped to strengthen the manuscript. A.L.S. acknowledges funding from the National Science Foundation Grant No. 1350580. Use of the Stanford Synchrotron Radiation Lightsource, SLAC National Accelerator Laboratory, is supported by the U.S. Department of Energy, Office of Science, Office of Basic Energy Sciences under Contract No. DE-AC02-76SF00515. The SSRL Structural Molecular Biology Program is supported by the DOE Office of Biological and Environmental Research, and by the National Institutes of Health, National Institute of General Medical Sciences (including P41GM103393). The contents of this publication are solely the responsibility of the authors and do not necessarily represent the official views of NIGMS or NIH.

Author Contributions: A.L.S. conceived the research, performed the experiments, and wrote the article with contributions from J.R. and S.M.W. Both S.M.W. and J.R. provided technical assistance to A.L.S. and contributed intellectually to experimental design.

Conflicts of Interest: The authors declare no conflicts of interest

References

1. Rahman, M.A.; Rahman, M.M.; Hasegawa, H. Arsenic-induced straighthead: An impending threat to sustainable rice production in south and south-east asia. *Bull. Environ. Contam. Toxicol.* **2012**, *88*, 311–315. [[CrossRef](#)] [[PubMed](#)]
2. Zhao, F.J.; Zhu, Y.G.; Meharg, A.A. Methylated arsenic species in rice: Geographical variation, origin, and uptake mechanisms. *Environ. Sci. Technol.* **2013**, *47*, 3957–3966. [[CrossRef](#)] [[PubMed](#)]
3. Zavala, Y.J.; Duxbury, J.M. Arsenic in rice: I. Estimating normal levels of total arsenic in rice grain. *Environ. Sci. Technol.* **2008**, *42*, 3856–3860. [[CrossRef](#)] [[PubMed](#)]
4. Williams, P.N.; Price, A.H.; Raab, A.; Hossain, S.A.; Feldmann, J.; Meharg, A.A. Variation in arsenic speciation and concentration in paddy rice related to dietary exposure. *Environ. Sci. Technol.* **2005**, *39*, 5531–5540. [[CrossRef](#)] [[PubMed](#)]
5. Meharg, A.A.; Macnair, M.R. Suppression of the high-affinity phosphate-uptake system—A mechanism of arsenate tolerance in *Holcus lanatus* L. *J. Exp. Bot.* **1992**, *43*, 519–524. [[CrossRef](#)]
6. Ma, J.F.; Yamaji, N.; Mitani, N.; Xu, X.-Y.; Su, Y.-H.; McGrath, S.P.; Zhao, F.-J. Transporters of arsenite in rice and their role in arsenic accumulation in rice grain. *Proc. Natl. Acad. Sci. USA* **2008**, *105*, 9931–9935. [[CrossRef](#)] [[PubMed](#)]
7. Li, R.Y.; Ago, Y.; Liu, W.J.; Mitani, N.; Feldmann, J.; McGrath, S.P.; Ma, J.F.; Zhao, F.J. The rice aquaporin *Isi1* mediates uptake of methylated arsenic species. *Plant Physiol.* **2009**, *150*, 2071–2080. [[CrossRef](#)] [[PubMed](#)]
8. Seyfferth, A.L.; Morris, A.H.; Gill, R.; Kearns, K.A.; Mann, J.N.; Paukett, M.; Leskani, C. Soil incorporation of silica-rich rice husk decreases inorganic arsenic in rice grain. *J. Agric. Food Chem.* **2016**, *64*, 3760–3766. [[CrossRef](#)] [[PubMed](#)]
9. Ma, R.; Shen, J.L.; Wu, J.S.; Tang, Z.; Shen, Q.R.; Zhao, F.J. Impact of agronomic practices on arsenic accumulation and speciation in rice grain. *Environ. Pollut.* **2014**, *194*, 217–223. [[CrossRef](#)] [[PubMed](#)]
10. Takahashi, Y.; Minamikawa, R.; Hattori, K.H.; Kurishima, K.; Kihou, N.; Yuita, K. Arsenic behavior in paddy fields during the cycle of flooded and non-flooded periods. *Environ. Sci. Technol.* **2004**, *38*, 1038–1044. [[CrossRef](#)] [[PubMed](#)]
11. Zhao, F.J.; McGrath, S.P.; Meharg, A.A. Arsenic as a food chain contaminant: Mechanisms of plant uptake and metabolism and mitigation strategies. *Annu. Rev. Plant Biol.* **2010**, *61*, 535–559. [[CrossRef](#)] [[PubMed](#)]
12. Marschner, H. *Mineral Nutrition of Higher Plants*, 2nd ed.; Academic Press: New York, NY, USA, 2003.
13. Ma, F.S.; Peterson, C.A. Current insights into the development, structure, and chemistry of the endodermis and exodermis of roots. *Can. J. Bot.* **2003**, *81*, 405–421. [[CrossRef](#)]
14. Enstone, D.E.; Peterson, C.A. The apoplastic permeability of root apices. *Can. J. Bot.* **1992**, *70*, 1502–1512. [[CrossRef](#)]
15. Hochholdinger, F.; Zimmermann, R. Conserved and diverse mechanisms in root development. *Curr. Opin. Plant Biol.* **2008**, *11*, 70–74. [[CrossRef](#)] [[PubMed](#)]
16. Huang, C.X.; Vansteveninck, R.F.M. The role of particular pericycle cells in apoplastic transport in root meristems of barley. *J. Plant Physiol.* **1990**, *135*, 554–558. [[CrossRef](#)]
17. Peterson, R.L.; Peterson, C.A. Ontogeny and anatomy of lateral roots. In *New Root Formation in Plants and Cuttings*; Jackson, M.B., Ed.; Springer: Dordrecht, The Netherlands, 1986; pp. 1–30.

18. Williams, P.N.; Santner, J.; Larsen, M.; Lehto, N.J.; Oburger, E.; Wenzel, W.; Glud, R.N.; Davison, W.; Zhang, H. Localized flux maxima of arsenic, lead, and iron around root apices in flooded lowland rice. *Environ. Sci. Technol.* **2014**, *48*, 8498–8506. [[CrossRef](#)] [[PubMed](#)]
19. Seyfferth, A.L.; Webb, S.M.; Andrews, J.C.; Fendorf, S. Arsenic localization, speciation, and co-occurrence with iron on rice (*Oryza sativa* L.) roots having variable Fe coatings. *Environ. Sci. Technol.* **2010**, *44*, 8108–8113. [[CrossRef](#)] [[PubMed](#)]
20. Kopittke, P.M.; de Jonge, M.D.; Wang, P.; McKenna, B.A.; Lombi, E.; Paterson, D.J.; Howard, D.L.; James, S.A.; Spiers, K.M.; Ryan, C.G.; et al. Laterally resolved speciation of arsenic in roots of wheat and rice using fluorescence-XANES imaging. *New Phytol.* **2014**, *201*, 1251–1262. [[CrossRef](#)] [[PubMed](#)]
21. Yamaguchi, N.; Ohkura, T.; Takahashi, Y.; Maejima, Y.; Arao, T. Arsenic distribution and speciation near rice roots influenced by iron plaques and redox conditions of the soil matrix. *Environ. Sci. Technol.* **2014**, *48*, 1549–1556. [[CrossRef](#)] [[PubMed](#)]
22. Wang, P.; Menzies, N.W.; Lombi, E.; McKenna, B.A.; James, S.; Tang, C.X.; Kopittke, P.M. Synchrotron-based X-ray absorption near-edge spectroscopy imaging for laterally resolved speciation of selenium in fresh roots and leaves of wheat and rice. *J. Exp. Bot.* **2015**, *66*, 4795–4806. [[CrossRef](#)] [[PubMed](#)]
23. Kopittke, P.M.; de Jonge, M.D.; Menzies, N.W.; Wang, P.; Donner, E.; McKenna, B.A.; Paterson, D.; Howard, D.L.; Lombi, E. Examination of the distribution of arsenic in hydrated and fresh cowpea roots using two- and three-dimensional techniques. *Plant Physiol.* **2012**, *159*, 1149–1158. [[CrossRef](#)] [[PubMed](#)]
24. Ma, J.F.; Goto, S.; Tamai, K.; Ichii, M. Role of root hairs and lateral roots in silicon uptake by rice. *Plant Physiol.* **2001**, *127*, 1773–1780. [[CrossRef](#)] [[PubMed](#)]
25. Chen, Y.; Sun, S.; Tang, Z.; Liu, G.; Moore, K.L.; Maathuis, F.J.M.; Miller, A.J.; McGrath, S.P.; Zhao, F.J. The nodulin 26-like intrinsic membrane protein OsNIP3;2 is involved in arsenite uptake by lateral roots in rice. *J. Exp. Bot.* **2017**, *68*, 3007–3016. [[CrossRef](#)] [[PubMed](#)]
26. Dixit, S.; Hering, J.G. Comparison of arsenic(V) and arsenic(III) sorption onto iron oxide minerals: Implications for arsenic mobility. *Environ. Sci. Technol.* **2003**, *37*, 4182–4189. [[CrossRef](#)] [[PubMed](#)]
27. Amaral, D.C.; Lopes, G.; Guilherme, L.R.G.; Seyfferth, A.L. A new approach to sampling intact Fe plaque reveals Si-induced changes in Fe mineral composition and shoot as in rice. *Environ. Sci. Technol.* **2017**, *51*, 38–45. [[CrossRef](#)] [[PubMed](#)]
28. Seyfferth, A.L. Abiotic effects of dissolved oxyanions on iron plaque quantity and mineral composition in a simulated rhizosphere. *Plant Soil* **2015**, *397*, 43–61. [[CrossRef](#)]
29. Seyfferth, A.L.; Webb, S.M.; Andrews, J.C.; Fendorf, S. Defining the distribution of arsenic species and plant nutrients in rice (*Oryza sativa* L.) from the root to the grain. *Geochim. Cosmochim. Acta* **2011**, *75*, 6655–6671. [[CrossRef](#)]
30. Clarkson, D.T.; Sanderson, J. Sites of absorption and translocation of iron in barley roots—Tracer and microautoradiographic studies. *Plant Physiol.* **1978**, *61*, 731–736. [[CrossRef](#)] [[PubMed](#)]
31. Marschner, H.; Romheld, V.; Kissel, M. Localization of phytosiderophore release and of iron uptake along intact barley roots. *Physiol. Plant* **1987**, *71*, 157–162.
32. Wang, P.; Menzies, N.W.; Lombi, E.; McKenna, B.A.; de Jonge, M.D.; Paterson, D.J.; Howard, D.L.; Glover, C.J.; James, S.; Kappen, P.; et al. In situ speciation and distribution of toxic selenium in hydrated roots of cowpea. *Plant Physiol.* **2013**, *163*, 407–418. [[CrossRef](#)] [[PubMed](#)]
33. Steudle, E.; Peterson, C.A. How does water get through roots? *J. Exp. Bot.* **1998**, *49*, 775–788. [[CrossRef](#)]
34. Yamaji, N.; Mitani, N.; Ma, J.F. A transporter regulating silicon distribution in rice shoots. *Plant Cell* **2008**, *20*, 1381–1389. [[CrossRef](#)] [[PubMed](#)]
35. Ma, J.F.; Yamaji, N.; Mitani, N.; Tamai, K.; Konishi, S.; Fujiwara, T.; Katsuhara, M.; Yano, M. An efflux transporter of silicon in rice. *Nature* **2007**, *448*, U209–U212. [[CrossRef](#)] [[PubMed](#)]
36. Moore, K.L.; Schroder, M.; Wu, Z.C.; Martin, B.G.H.; Hawes, C.R.; McGrath, S.P.; Hawkesford, M.J.; Ma, J.F.; Zhao, F.J.; Grovenor, C.R.M. High-resolution secondary ion mass spectrometry reveals the contrasting subcellular distribution of arsenic and silicon in rice roots. *Plant Physiol.* **2011**, *156*, 913–924. [[CrossRef](#)] [[PubMed](#)]
37. Moore, K.L.; Chen, Y.; van de Meene, A.M.L.; Hughes, L.; Liu, W.J.; Geraki, T.; Mosselmans, F.; McGrath, S.P.; Grovenor, C.; Zhao, F.J. Combined nanosims and synchrotron X-ray fluorescence reveal distinct cellular and subcellular distribution patterns of trace elements in rice tissues. *New Phytol.* **2014**, *201*, 104–115. [[CrossRef](#)] [[PubMed](#)]

38. Zhao, F.J.; Ma, J.F.; Meharg, A.A.; McGrath, S.P. Arsenic uptake and metabolism in plants. *New Phytol.* **2009**, *181*, 777–794. [[CrossRef](#)] [[PubMed](#)]
39. Carey, A.M.; Scheckel, K.G.; Lombi, E.; Newville, M.; Choi, Y.; Norton, G.J.; Charnock, J.M.; Feldmann, J.; Price, A.H.; Meharg, A.A. Grain unloading of arsenic species in rice. *Plant Physiol.* **2010**, *152*, 309–319. [[CrossRef](#)] [[PubMed](#)]
40. Seyfferth, A.L.; Fendorf, S. Silicate mineral impacts on the uptake and storage of arsenic and plant nutrients in rice (*Oryza sativa* L.). *Environ. Sci. Technol.* **2012**, *46*, 13176–13183. [[CrossRef](#)] [[PubMed](#)]
41. Roberts, L.C.; Hug, S.J.; Dittmar, J.; Voegelin, A.; Saha, G.C.; Ali, M.A.; Badruzzanian, A.B.M.; Kretzschmar, R. Spatial distribution and temporal variability of arsenic in irrigated rice fields in bangladesh. 1. Irrigation water. *Environ. Sci. Technol.* **2007**, *41*, 5960–5966. [[CrossRef](#)] [[PubMed](#)]
42. Pedler, J.F.; Parker, D.R.; Crowley, D.E. Zinc deficiency-induced phyto siderophore release by the triticeae is not consistently expressed in solution culture. *Planta* **2000**, *211*, 120–126. [[CrossRef](#)] [[PubMed](#)]
43. Seyfferth, A.L.; Parker, D.R. Effects of genotype and transpiration rate on the uptake and accumulation of perchlorate (ClO_4^-) in lettuce. *Environ. Sci. Technol.* **2007**, *41*, 3361–3367. [[CrossRef](#)] [[PubMed](#)]
44. Brundrett, M.C.; Enstone, D.E.; Peterson, C.A. A berberine-aniline blue fluorescent staining procedure for suberin, lignin, and callose in plant-tissue. *Protoplasma* **1988**, *146*, 133–142. [[CrossRef](#)]
45. Webb, S.M. The Microanalysis Toolkit: X-ray Fluorescence Image Processing Software. *Am. Inst. Phys. Conf. Proc.* **2011**, *1365*, 196–199.



© 2017 by the authors. Licensee MDPI, Basel, Switzerland. This article is an open access article distributed under the terms and conditions of the Creative Commons Attribution (CC BY) license (<http://creativecommons.org/licenses/by/4.0/>).